Supporting Information

Single-cell Thermometry with a Nanothermocouple Probe

Li-Qiu Huang, Xin-Lei Ding, Xiao-Tong Pan, Zhong-Qiu Li*, Kang Wang, Xing-Hua Xia*

State Key Laboratory of Analytical Chemistry for Life Science, School of Chemistry and Chemical Engineering, Nanjing University, Nanjing, 210093, China.

E-mail: zhongqiuli@nju.edu.cn; xhxia@nju.edu.cn

Contents

Experimental Section

Materials and reagents

Quartz capillaries (outer diameter: 1.0 mm; inner diameter: 0.7 mm; length: 10 cm) were purchased from Sutter Instrument (USA). $[Ru(NH_3)_6]Cl_3$ was purchased from Bide Pharmatech Ltd. (China). Sliver wires (Φ:0.2mm) and glucose were purchased from Sinopharm Chemical Reagent Co., Ltd. (China). $MgCl_2 \cdot 6H_2O$ was purchased from Xilong Scientific Co., Ltd. (China). Bovine Serum Albumin (BSA), $H_2PtCl_6 \cdot 6H_2O$, L-Ascorbic acid (L-AA) and L-Glutathione reduced (L-GSH) were purchased from Sigma-Aldrich (USA). 30 wt. % H_2O_2 and $CaCl_2$ were purchased from Aladdin Biochemical Technology Co., Ltd. (China). 0.01 M phosphate buffered saline (PBS, pH 7.4), RPMI-1640 medium, Dulbecco's modified eagle medium (DMEM), Hoechst 33342/Propidium iodide (PI) double fluorescence staining kit, 4% paraformaldehyde, human breast cancer cells (MCF-7) and human normal liver cells (LO2) were purchased from Jiangsu KeyGen Biotech. Co., Ltd. (China). Fetal Bovine Serum (FBS) was purchased from Gibco (USA). Carbonyl cyanide 4-(trifluoromethoxy) phenylhydrazone (FCCP) was purchased from Glpbio (USA). Camptothecin (CPT) was purchased from HEOWNS Biochem Technologies Co., Ltd. (China). Doxorubicin (DOX) was purchased from Hefei Bomei Biotechnology Co., Ltd. (China). 3D MCF7 Cell Culture Models were purchased from Jiangsu Avatarget Biotechnology Co., Ltd. (China). All aqueous solutions were prepared from deionized water (Millipore, 18 MΩ cm).

Experimental setup and data acquisition

The nanopipettes were pulled using a P-2000 laser micropuller (Sutter Instruments, USA). The pyrolytic carbon deposition was performed on a home-made setup. All electrochemical tests were performed on a CHI 660d electrochemical workstation (CH Instruments Inc., China). The sputtering of platinum was performed on a high vacuum coating system ACE600 (Leica Co., Ltd., Germany). Scanning electron microscopy (SEM) was carried out on a JEOL JSM-7800F scanning electron

microscope (JEOL Japan Electronics Co., Ltd., Japan). The focused ion beam (FIB) as well as the following SEM imaging and Energy-dispersive X-ray spectroscopy (EDS) mapping were performed on a Helios 600i Dual Beam Scanning Electron Microscope (FEI Co., Ltd., USA). Thermoelectric signals of nanothermocouple probes were recorded by a DMM7510 digital multimeter (Keithley Instruments, USA). Temperature controlling experiments were performed with a VIVO iTherm water bath circulation system (Julabo Labortechnik GmbH, Germany) and a TSP01 USB temperature Data Logger (Thorlabs Inc., USA). A laser beam with wavelength of 405 nm and output power of 0.5 W (Shanghai Zhuolong Electronics Co., LTD, China) was used for laser test. During intracellular tests, the nanothermocouple probes were manipulated by a PCS-5000 motorized patch-clamp micromanipulator (Thorlabs Inc., USA) to target single cells or 3D cell culture models with the assistance of a Nikon Eclipse Ti inverted fluorescence microscope (Nikon Co., Ltd., Japan).

Fabrication and characterization of C/Pt nanothermocouple probes

As shown in Figure S1 and S2, two ends of the quartz capillaries were first deposited with carbon by butane pyrolysis with argon gas protection.[1] The flow rate of argon and butane gas was *ca*.10 mL/min and the deposition time was 1 min for each end. Then, the deposited quartz capillaries were cleaned by a plasma cleaner to remove residual organic impurities on the surface before being pulled to nanopipettes. A two-line program was used for pulling: LINE1: HEAT = 775, FIL = 4, VEL = 36, DEL = 190; LINE2: HEAT = 745, FIL = 4, VEL = 34, DEL = 160, PUL = 230. Aperture of the obtained nanopipetts was *ca*.145 nm.

The tip of the as-prepared nanopipette was also deposited with carbon for 2.5 min. Electrical contact of the inner carbon layer and the diameter of carbon exposed at the orifice were characterized by cyclic voltammetry (CV) in a 5 mM $[Ru(NH_3)_6]Cl_3$ aqueous solution. A two-electrode configuration was used for the CV test, in which a Ag/AgCl wire electrode was employed as a reference/counter electrode. The CVs were collected in a potential range from 0.3 V to -0.5 V at a scan rate of 0.01 V/s.

Subsequently, the electrodeposition of a thin-layer platinum on the carbon exposed

at the orifice of the nanopipette was conducted by CV in a 2 mM H_2PtCl_6 aqueous solution to form the carbon-platinum heterojunctions.[2] A three-electrode configuration with a platinum wire as a counter electrode and a Ag/AgCl (3 M KCl) electrode as reference was used. The CVs were recorded in a potential range from 0.3 V to -0.5 V at a scan rate of 0.2 V/s. Magnetron sputtering of platinum was further performed with two steps: first, the nanopipette was faced toward the sputter source following by a 30-s sputtering; second, the nanopipette was positioned parallel to the sputter source following by a 10-min sputtering to ensure the full coverage of platinum on the outer surface. Then, silver wires were attached to the external platinum layer and internal carbon layer at the tail end of the pipette, respectively.

In order to investigate the internal structure of the nanothermocouple probe, the as-prepared C/Pt nanothermocouple probe was cut apart in an axial direction by FIB. SEM characterization and EDS mapping of the slice were then performed.

Evaluation of temperature sensing properties

To evaluate temperature sensing properties of the nanothermocouple probe, the tip of as-prepared nanothermocouple probe was immersed in an electrochemical cell filled with 10 mM PBS (pH 7.4). Two silver wires attached to the tail end of the nanothermocouple probe were connected to a digital multimeter. The temperature of PBS was precisely controlled. During the calibration of the nanothermocouple probe, the solution temperature, which is designated as the temperature of the hot end (T_h), was recorded by one probe of the commercial thermometer. The room temperature, which is designated as the temperature of the cold end (T_c), was recorded by another probe of the commercial thermometer.

Cell culture and treatment

MCF7 and LO2 cells were cultured in RPMI-1640 medium with 10% (v/v) FBS, 80 U/mL penicillin and 0.08 mg/mL streptomycin. 3D MCF7 cell culture models were cultured in DMEM with 10% FBS, 80 U/mL penicillin and 0.08mg/mL streptomycin. All cells were incubated with 5% CO_2 in a humidified chamber at 37 °C. The fixation

of cells was performed with 4% paraformaldehyde according to the standard protocol. The viability of cells and the integrity of their membranes were verified by Hoechst 33342/ PI double fluorescence staining kit. The cells were stained by these two dyes according to the instructions.

Studies of single cells and 3D Cell culture models (3D-CCMs)

For intracellular experiments, the nanothermocouple probe was fixed to the holder integrated with a micromanipulator and an inverted fluorescence microscope. The cells were rinsed with 10 mM PBS (pH 7.4) buffer before tests. The penetration of the nanothermocouple probe into the cells was monitored by the microscope and the digital multimeter simultaneously. The nanothermocouple probe was first controlled with coarse movement and then switched to fine movement when approaching the cell under a 60x objective. Upon penetration, a prompt increase of the thermoelectric reading and a slight shake of the cell can be observed, indicating that the tip has successfully entered the cell.

Drug treatment was performed after the reading of the multimeter reached a balanced state. The concentrated solutions of three drugs, including FCCP, CPT and DOX, were respectively added to the cell culture dishes filled with 10 mM PBS to stimulate the target cells. The temperature of the adding solutions was adjusted to the same as cell buffers in advance.

As for the experiments of 3D-CCMs, the main setup was kept the same as intracellular experiments. To measure the temperature gradients in a 3D-CCM, the nanothermocouple probe was first inserted into the edge of 3D-CCM and kept for a while to reach a balanced state. Then, the tip gradually went deeper into the 3D-CCM under the manipulation of the 3D micromanipulator.

During above measuring process, the room temperature was kept steady and monitored with the commercial thermometer.

Fabrication process of a C/Pt nanothermocouple probe

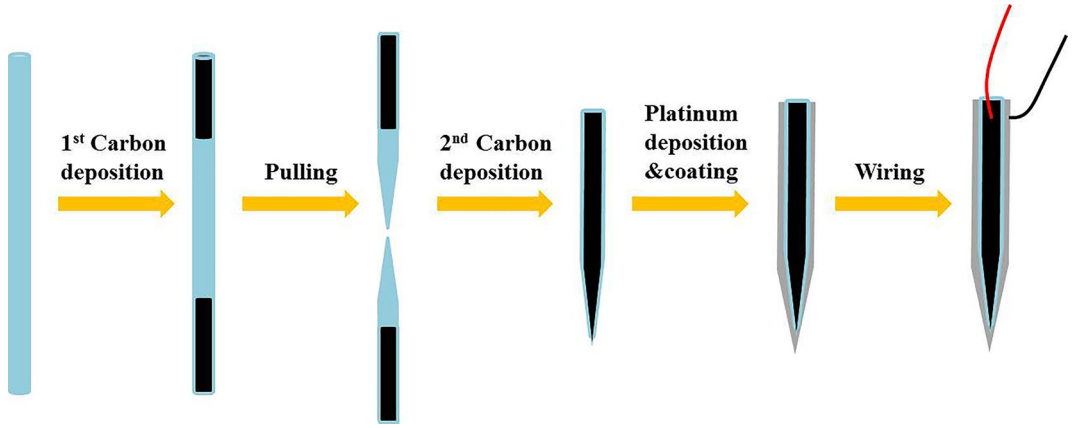

Figure S1. Schematic diagram of the fabrication process of C/Pt nanothermocouple probe.

Setup for carbon deposition

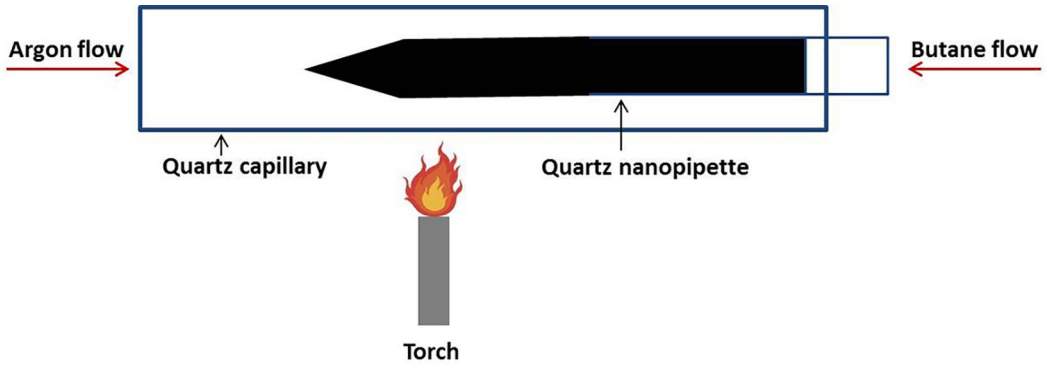

Figure S2. Schematic diagram of the carbon deposition setup.

Basic principles of the nanothermocouple probe

The thermometric property of the nanothermocouple probe is based on Seebeck effect, which refers to a thermoelectric potential induced by a temperature difference between two conductors/semiconductors. As shown in Figure S3, a typical thermocouple consists of two different conducting materials. One end of them comes into contact with each other to form an electrical junction, called the hot end. While the other end is separately connected to a voltage measuring device, called the cold end. The hot end serves as the temperature sensing region and the cold end serves as the temperature reference region. The voltage across a thermocouple (E_T) is given by: [5]

$$E_T = (S_A - S_B)(T_h - T_c) = \Delta S \cdot \Delta T \qquad \text{(S1)}$$

where S_A and S_B are the Seebeck coefficients of the two conducting materials used in the thermocouple, T_h is the temperature of the hot end, and T_c is the temperature of the cold end.

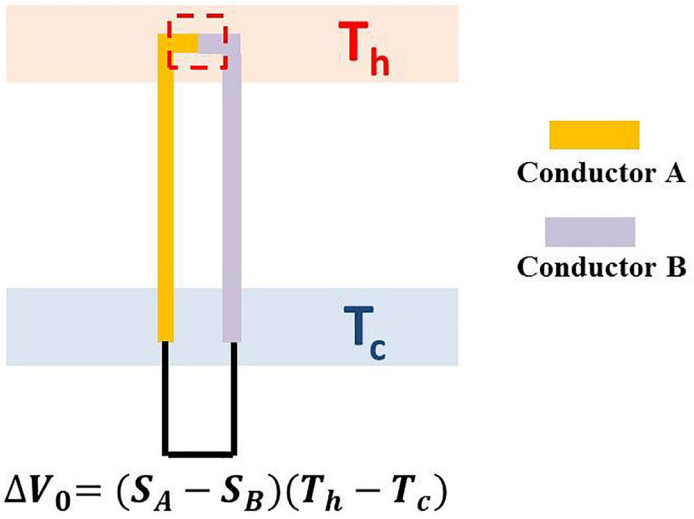

Figure S3. Schematic diagram of a typical thermocouple.

SEM characterization of the C/Pt nanothermocouple probe

The top-view scanning electron microscopy (SEM) images exhibit the morphologies of the nanopipette at each fabrication stage.

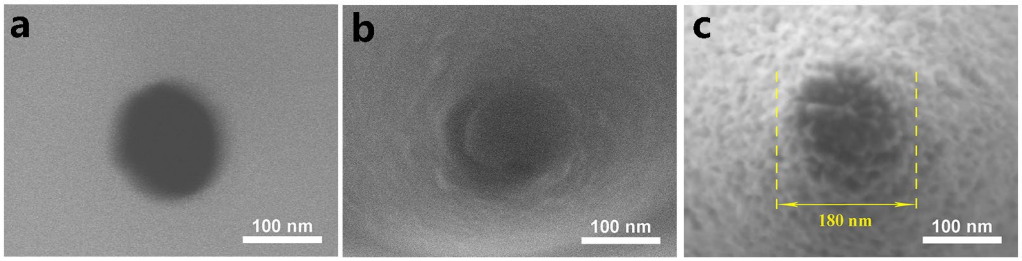

Figure S4. Top-view SEM images of (a) the pristine quartz nanopipette with an orifice of ca. 145 nm, (b) the nanopipette after internal carbon deposition, (c) the nanopipette after external platinum deposition.

CV characterization of the carbon deposited in the orifice

The electrical contact of the inner carbon layer and the diameter of carbon exposed at the orifice was characterized by cyclic voltammetry (CV) in a 5 mM $[Ru(NH_3)_6]Cl_3$ aqueous solution. As shown in Figure S5, the current for the one-electron reduction of $[Ru(NH_3)_6]^{3+}$ shows a typical sigmoidal response, demonstrating a good electrical contact of the inner carbon layer and characteristic microelectrode properties. The steady-state current is about -113 pA. The size of the carbon electrode was calculated according to the following formula:[3]

$$I_{ss} = 2.57n\mathrm{FDcd} \qquad \text{(S2)}$$

where I_{ss} is the steady-state current, n is the number of transferred electrons, F is the Faraday constant, D is the diffusion coefficient ($5.5*10^{-6}$ cm^2/s),[4] c is the bulk concentration of the redox species, and d is the tip diameter. The diameter of the carbon exposed at the orifice was estimated to be 166 nm from the steady-state current.

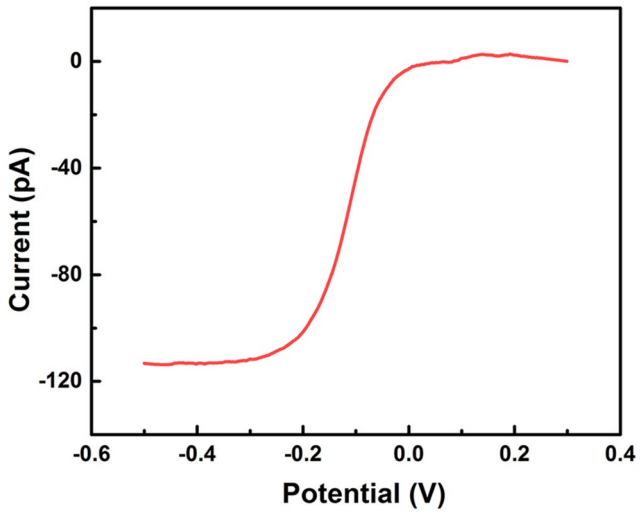

Figure S5. CV of the carbon electrode deposited on nanopipette in a 5 mM $Ru(NH_3)_6Cl_3$ aqueous solution at a scan rate of 0.01V/s.

Optical image and EDS mapping of the C/Pt nanothermocouple probe

The optical image shows that the fabricated nanothermocouple probe is about 5 cm in length with an extremely sharp tip (Figure S6a). The corresponding EDS elemental mapping of the nanothermocouple probe cut apart by FIB shows the presence of C, Si and Pt element at the probe tip, which corresponds to the three layers of deposited carbon, quartz wall and sputtered platinum, respectively (Figure S6b).

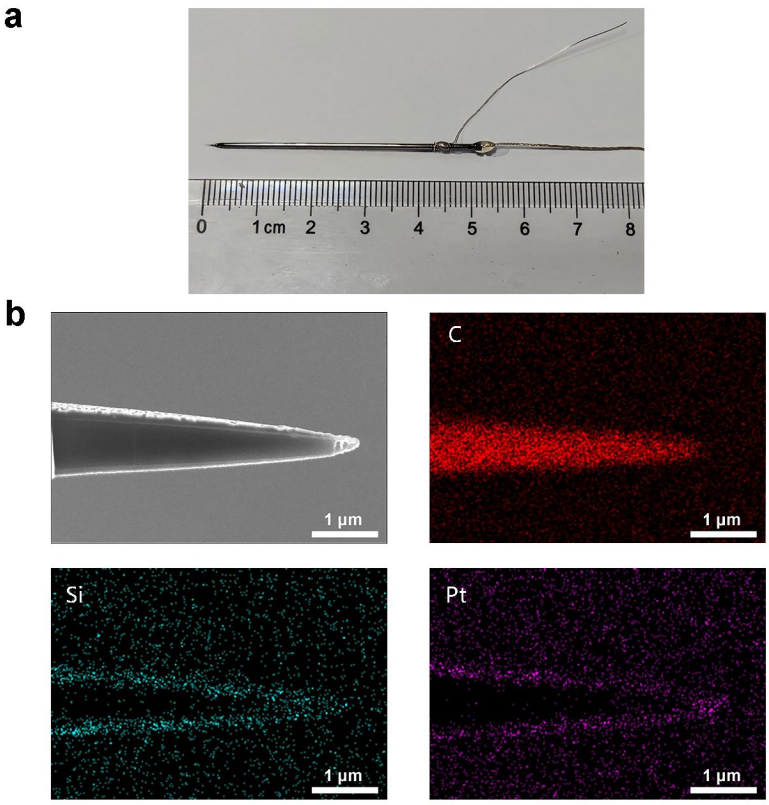

Figure S6. (a) Optical image of a C/Pt nanothermocouple probe. (b) Side-view SEM image of a nanothermocouple probe cut apart by FIB and the corresponding EDS mapping results.

Temperature resolution of the C/Pt nanothermocouple probe

The temperature resolution (δT) was calculated based on the calibration curve in Figure 2a by the following formula: [6]

$$\delta T = \left(\frac{\partial \Delta T}{\partial E_T}\right)\delta E_T \qquad \text{(S3)}$$

where $\left(\frac{\partial \Delta T}{\partial E_T}\right)$ and δE_T represent the inverse of the slope of the calibration curve and the corresponding standard deviation of the thermoelectric potential at each point, respectively. The calculated result is shown in Figure S7, which displays that the temperature resolution is 0.08-0.24 °C in the range of ΔT= -10-20 °C. The average value is 0.16 °C.

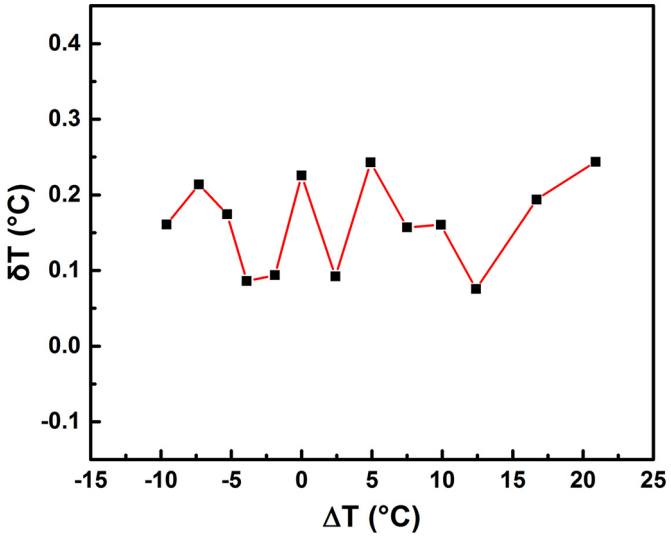

Figure S7. Temperature resolutions of the nanothermocouple probe at different temperature differences.

Characterization of the reversibility of the C/Pt nanothermocouple probe

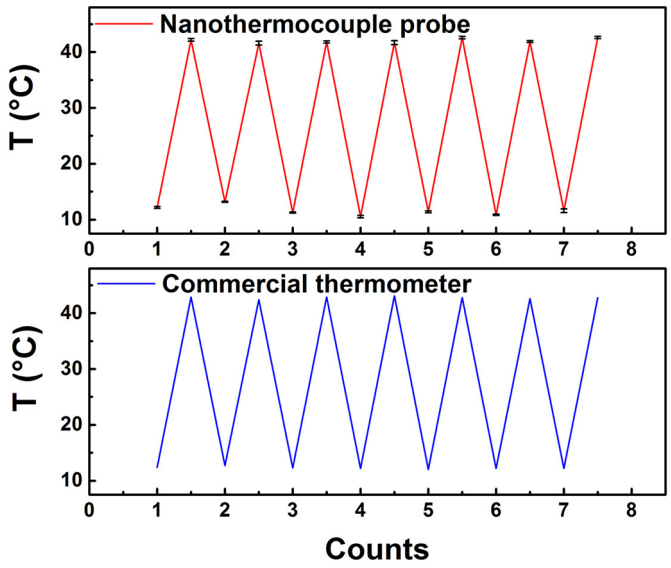

Figure S8. Characterization of the reversibility of the nanothermocouple probe. The temperature of PBS was switched between 12 °C and 42 °C for seven cycles during the test.

Characterization of the stability of the C/Pt nanothermocouple probe

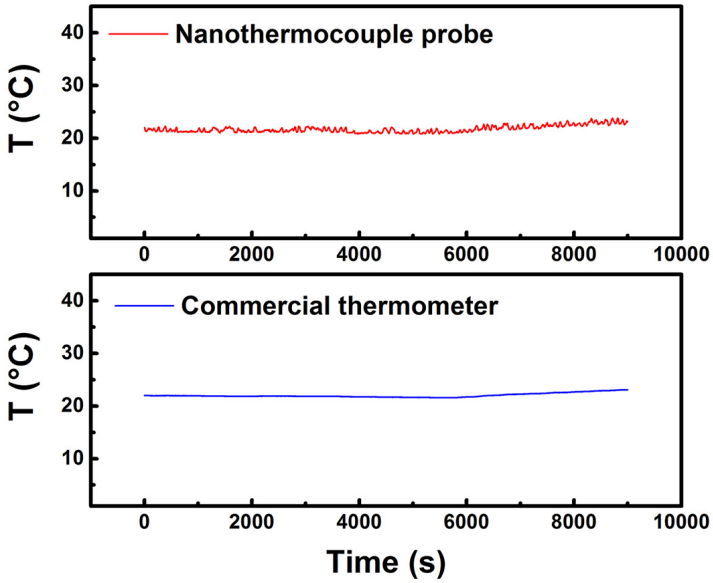

Figure S9. Characterization of the stability of the nanothermocouple probe. The temperature of PBS was kept near 22 °C during a continuous test of 9000 s.

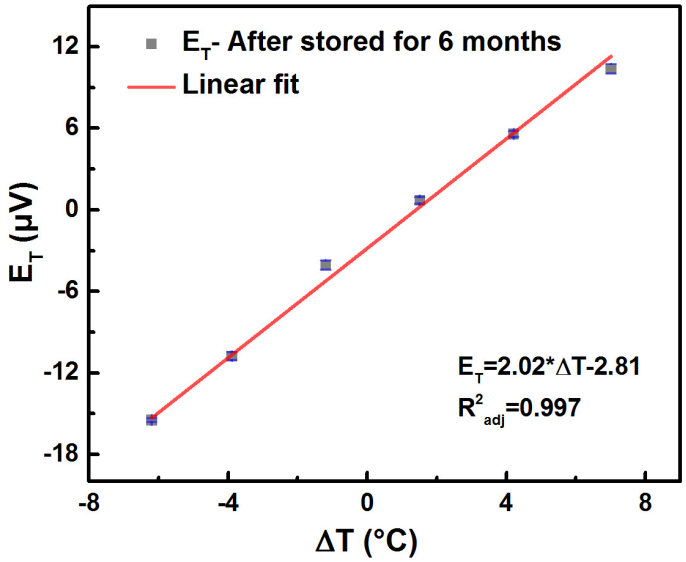

Figure S10. The calibration curve of a C/Pt nanothermocouple probe which has been stored in a plastic dish for six months. Each point was obtained by averaging one hundred original data points.

Characterization of the response speed of the C/Pt nanothermocouple probe

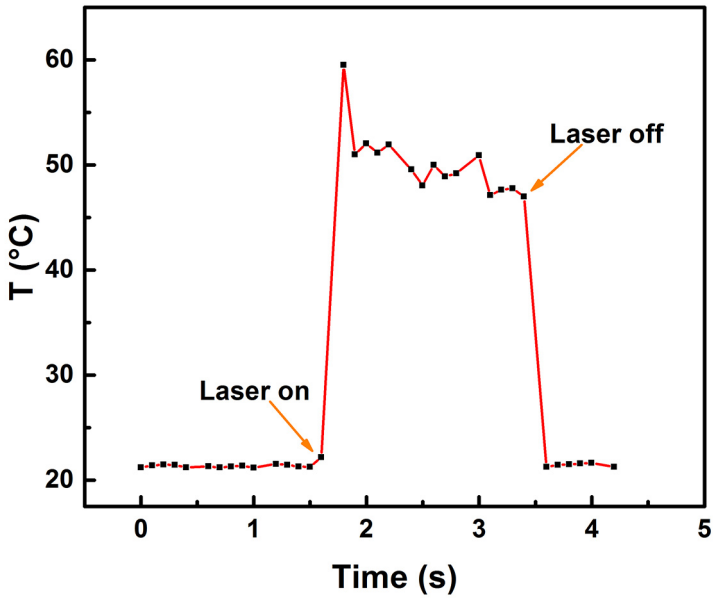

Figure S11. Magnified plot of the first cycle of the temperature variation caused by periodical laser heating of the tip in figure2d.

Characterization of the anti-interference capability of the C/Pt nanothermocouple probe

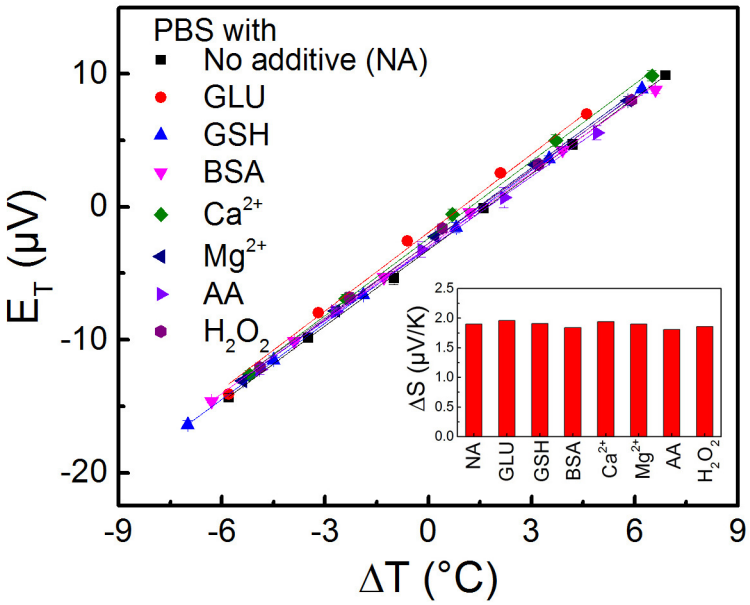

Figure S12. Calibration curves of the nanothermocouple probe in 10 mM PBS with various additives: glucose (GLU) of 10 mM level; glutathione (GSH), Ca^{2+}, Mg^{2+}, ascorbic acid (AA), and H_2O_2 of 1 mM level; 1.0% (w/v) bovine serum albumin (BSA) chosen to simulate the protein species. Inset: the corresponding thermoelectric coefficients.

Temperature sensing of LO2 cells

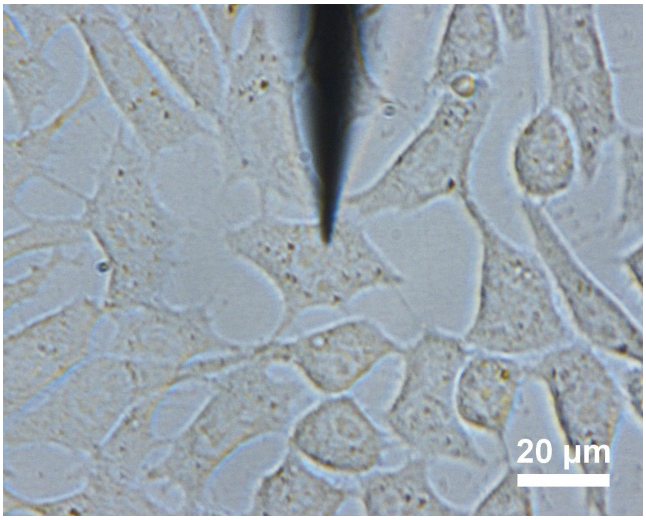

Figure S13. The bright-field image of LO2 cells after the penetration of a nanothermocouple probe.

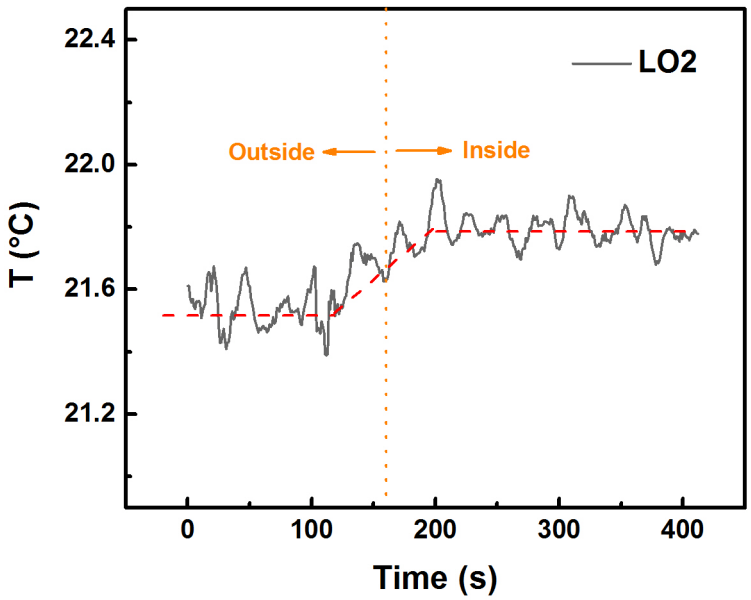

Figure S14. Temperature variations during the probe penetration into a living LO2 cell.

Continuous bright-field images of MCF7 cells

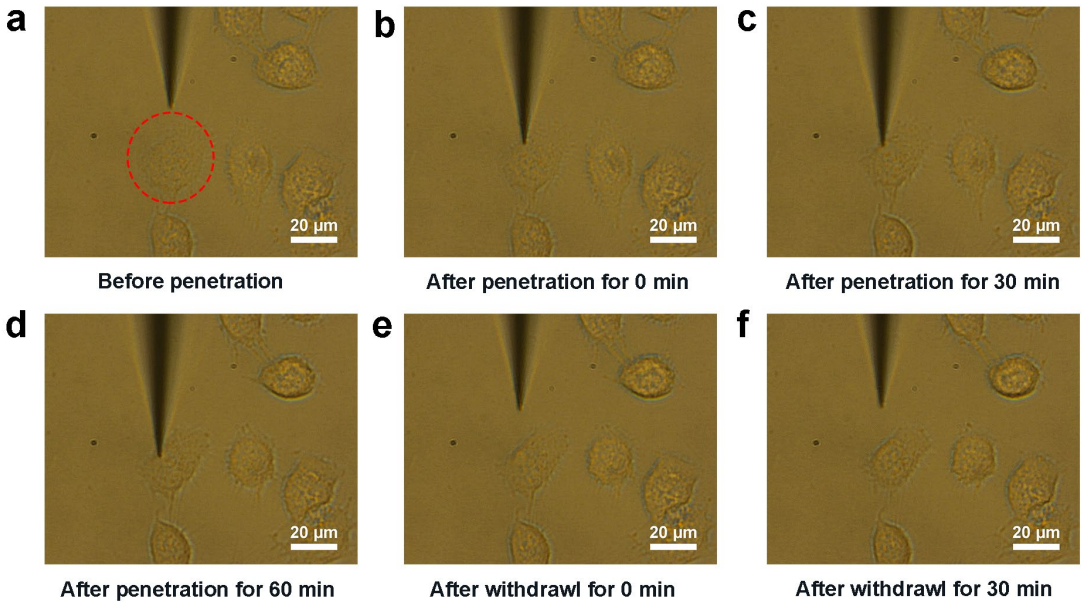

Figure S15. Continuous bright-field images of the morphology of the MCF7 cell (a) before penetration, (b) after penetration for 0 min, (c) after penetration for 30 min, (d) after penetration for 60 min, (e) after withdrawal for 0 min, (f) after withdrawal for 30 min.

Bright-field and fluorescence images of living/fixed MCF cells stained with Hoechst 33342 and PI

As shown in Figure S16, double staining experiment with Hoechst 33342 and Propidium iodide (PI) was conducted to confirm the cell viability after being penetrated with the nanothermocouple probe. MCF7 cells fixed by 4% paraformaldehyde were taken as control.

The Hoechst 33342 dye can slightly permeate into living cells, exhibiting weak blue fluorescence.[7] While for dead cells, the fluorescence intensity would be elevated as a result of the enhanced membrane permeability and structural transformation, exhibiting bright blue fluorescence. The PI dye can only permeate into leaked cells, leading to characteristic red fluorescence.[8] With the same exposure time, characteristic fluorescence was observed for fixed cells, indicating their death. While no obvious fluorescence was observed for the living MCF7 cell was observed after penetration for 80 min, indicating the viability and good membrane integrity of the cell.

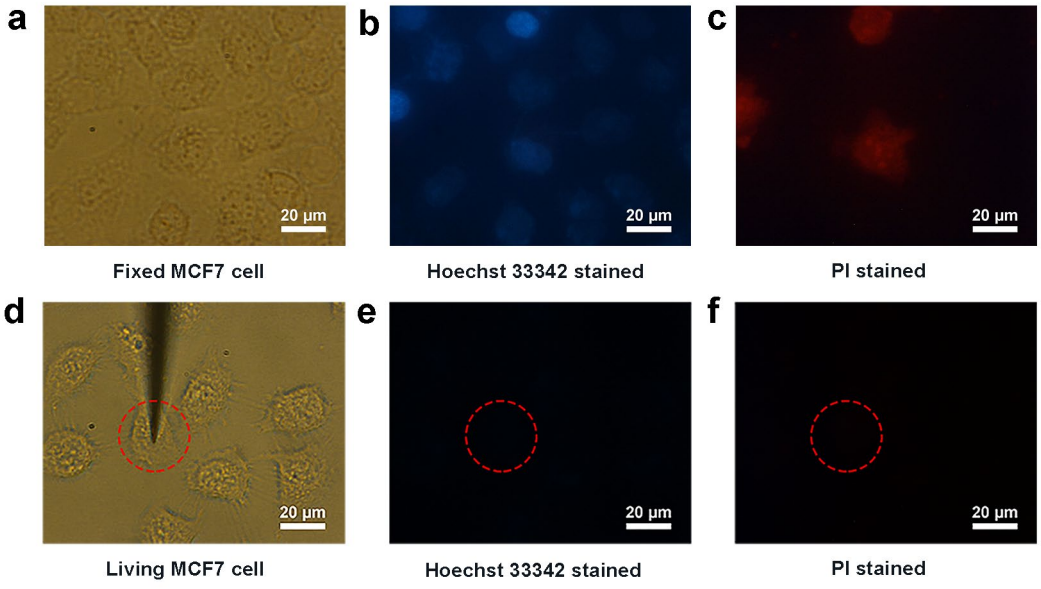

Figure S16. Bright-field and fluorescence images of living and fixed MCF7 cells stained with Hoechst 33342 and PI. (a-c) Bright-field and fluorescence images of fixed MCF7 cells. (d-f) Bright-field and fluorescence images of the living MCF7 cell after penetration for 80 min. The exposure time and excitation wavelength were 400 ms and 352 nm for (b) and (e), respectively. The exposure time and excitation wavelength were 2 s and 488 nm for (c) and (f), respectively.

Temperature Responses of single MCF7 cells to Drug Stimuli

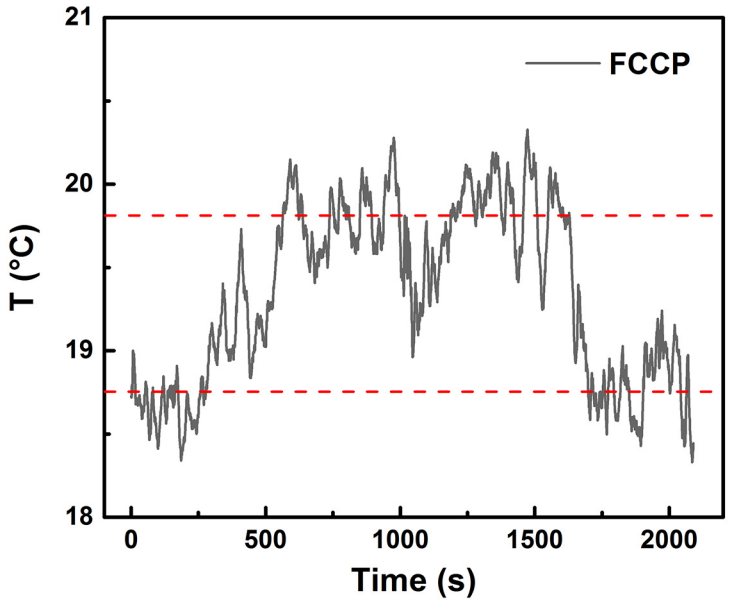

Figure S17. Temperature variations of the MCF7 cell with the addition of FCCP.

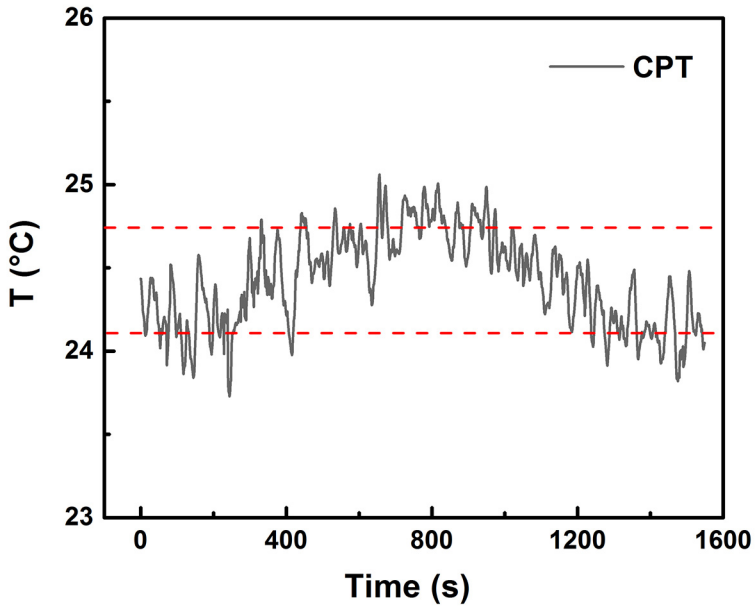

Figure S18. Temperature variations of the MCF7 cell with the addition of CPT.

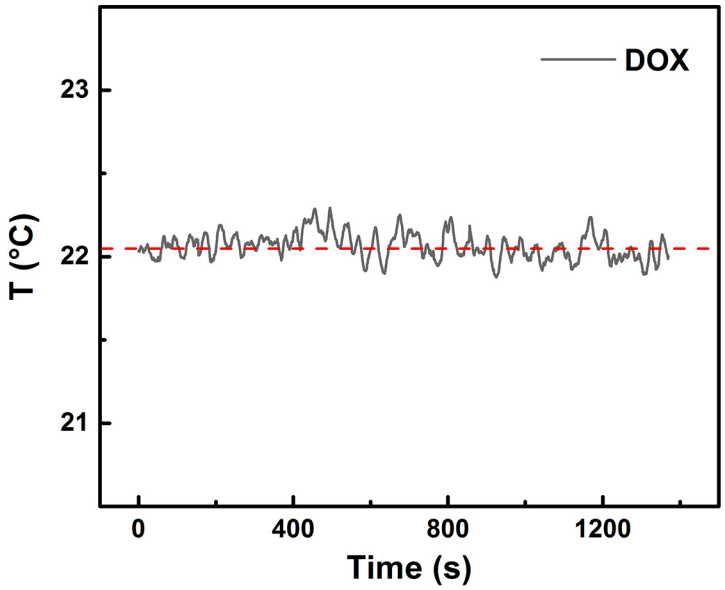

Figure S19. Temperature variations of the MCF7 cell with the addition of DOX.

Temperature Responses of single LO2 cells to Drug Stimuli

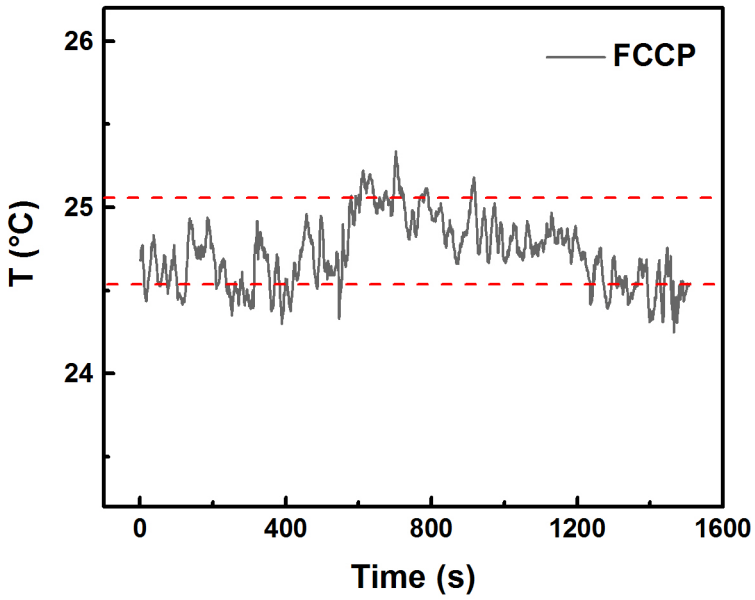

Figure S20. Temperature variations of the LO2 cell with the addition of FCCP.

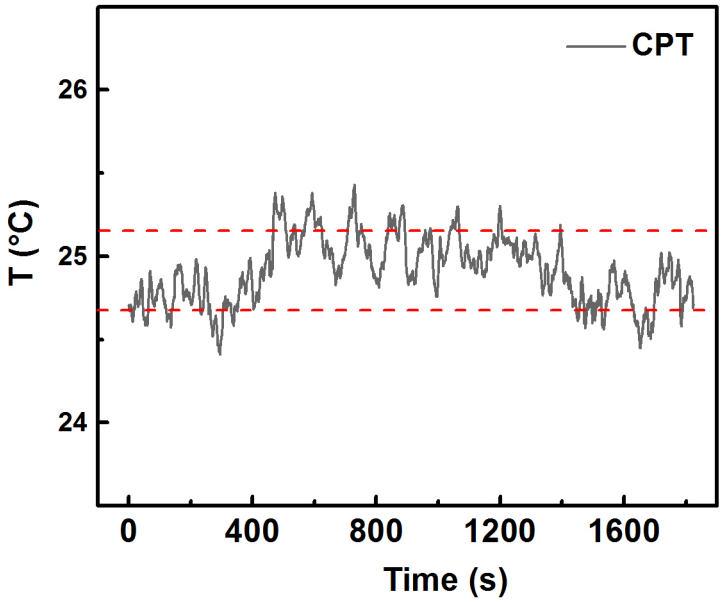

Figure S21. Temperature variations of the LO2 cell with the addition of CPT.

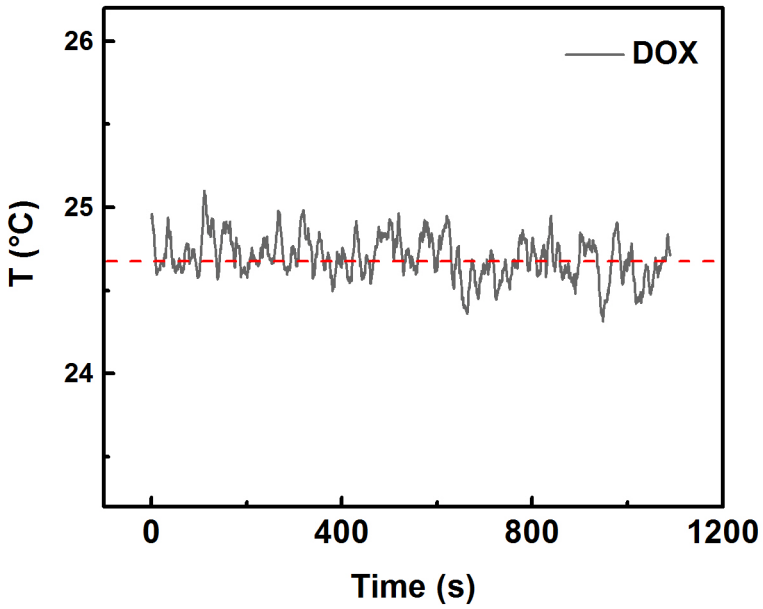

Figure S22. Temperature variations of the LO2 cell with the addition of DOX.

Reference

1. Wang, M. H.; Liu, J. J.; Liang, X.; Gao, R. Y.; Zhou, Y. M.; Nie, X.; Shao, Y.; Guan, Y.; Fu, L. M.; Zhang, J. P.; Shao, Y. H., Electrochemiluminescence based on a dual carbon ultramicroelectrode with confined steady-state annihilation. *Anal. Chem.* **2021,** *93*, 4528-4535.

2. Nebel, M.; Grützke, S.; Diab, N.; Schulte, A.; Schuhmann, W., Visualization of Oxygen Consumption of Single Living Cells by Scanning Electrochemical Microscopy: The Influence of the Faradaic Tip Reaction. Angew. Chem. Int. Ed. **2013**, *52*, 6335 –6338.

3. Takahashi, Y.; Shevchuk, A. I.; Novak, P.; Zhang, Y.; Ebejer, N.; Macpherson, J. V.; Unwin, P. R.; Pollard, A. J.; Roy, D.; Clifford, C. A.; Shiku, H.; Matsue, T.; Klenerman, D.; Korchev, Y. E., Multifunctional Nanoprobes for Nanoscale Chemical Imaging and Localized Chemical Delivery at Surfaces and Interfaces. *Angew. Chem.Int. Ed.* **2011**, *50*, 9638−9642.

4. Wipf, D. O.; Kristensen, E. W.; Deakin, M. R.; Wightman, R. M., Fast-Scan Cyclic Voltammetry as a Method To Measure Rapid, Heterogeneous Electron-Transfer Kinetics. *Anal. Chem.* **1988**, *60*, 306−310.

5. Bae, J.; Zheng, J. J.; Zhang, H. T.; Foster, P. J.; Needleman, D. J.; Vlassak, J. J., A micromachined picocalorimeter sensor for liquid samples with application to chemical reactions and biochemistry. *Adv. Sci.* **2021,** *8*, 11.

6. Okabe, K.; Inada, N.; Gota, C.; Harada, Y.; Funatsu, T.; Uchiyama, S., Intracellular temperature mapping with a fluorescent polymeric thermometer and fluorescence lifetime imaging microscopy. *Nat. Commun.* **2012,** *3*,1-9.

7. Crowley, L. C.; Marfell, B. J.; Waterhouse, N. J., Analyzing cell death by nuclear staining with Hoechst 33342. *Cold Spring Harb Protoc.* **2016**, *2016*, 778-781.

8. Wang, J. G.; Zhang, J. B.; Lee, Y. M.; Ng, S.; Shi, Y.; Hua, Z. C.; Lin, Q. S.; Shen, H. M., Nonradioactive quantification of autophagic protein degradation with (L)-azidohomoalanine labeling. *Nat. Protoc.* **2017,** *12*, 279-288.